blood®
Regular Article

LYMPHOID NEOPLASIA

Preclinical characterization of pirtobrutinib, a highly selective, noncovalent (reversible) BTK inhibitor

Eliana B. Gomez,[1,*] Kevin Ebata,[2,*] Hetal S. Randeria,[2] Mary S. Rosendahl,[1] E. Peder Cedervall,[1] Tony H. Morales,[1] Lauren M. Hanson,[1] Nicholas E. Brown,[3] Xueqian Gong,[3] Jennifer Stephens,[3] Wenjuan Wu,[3] Isabel Lippincott,[1] Karin S. Ku,[2] Richard A. Walgren,[3] Paolo B. Abada,[3] Joshua A. Ballard,[1] Charles K. Allerston,[1] and Barbara J. Brandhuber[1]

[1]Loxo@Lilly, Louisville, CO; [2]Loxo@Lilly, South San Francisco, CA; and [3]Loxo@Lilly, Indianapolis, IN

KEY POINTS

- **Pirtobrutinib is a potent, noncovalent (reversible), highly selective inhibitor of BTK and C481-mutant BTK.**
- **Pirtobrutinib is efficacious in B-cell models in vitro and in vivo, including patient-derived CLL cells.**

Bruton tyrosine kinase (BTK), a nonreceptor tyrosine kinase, is a major therapeutic target for B-cell–driven malignancies. However, approved covalent BTK inhibitors (cBTKis) are associated with treatment limitations because of off-target side effects, suboptimal oral pharmacology, and development of resistance mutations (eg, C481) that prevent inhibitor binding. Here, we describe the preclinical profile of pirtobrutinib, a potent, highly selective, noncovalent (reversible) BTK inhibitor. Pirtobrutinib binds BTK with an extensive network of interactions to BTK and water molecules in the adenosine triphosphate binding region and shows no direct interaction with C481. Consequently, pirtobrutinib inhibits both BTK and BTK C481 substitution mutants in enzymatic and cell-based assays with similar potencies. In differential scanning fluorimetry studies, BTK bound to pirtobrutinib exhibited a higher melting temperature than cBTKi-bound BTK. Pirtobrutinib, but not cBTKis, prevented Y551 phosphorylation in the activation loop. These data suggest that pirtobrutinib uniquely stabilizes BTK in a closed, inactive conformation. Pirtobrutinib inhibits BTK signaling and cell proliferation in multiple B-cell lymphoma cell lines, and significantly inhibits tumor growth in human lymphoma xenografts in vivo. Enzymatic profiling showed that pirtobrutinib was highly selective for BTK in >98% of the human kinome, and in follow-up cellular studies pirtobrutinib retained >100-fold selectivity over other tested kinases. Collectively, these findings suggest that pirtobrutinib represents a novel BTK inhibitor with improved selectivity and unique pharmacologic, biophysical, and structural attributes with the potential to treat B-cell–driven cancers with improved precision and tolerability. Pirtobrutinib is being tested in phase 3 clinical studies for a variety of B-cell malignancies.

Introduction

Bruton tyrosine kinase (BTK), a multidomain protein with pleckstrin homology, Tec homology, SRC homology (SH) 3, SH2, and kinase domains, is a critical component of the B-cell receptor signaling complex. BTK is activated by SRC family kinases phosphorylating BTK tyrosine 551 (Y551) in the kinase activation loop, leading to increased autophosphorylation of Y223 in the SH3 domain.[1] BTK regulates proliferation and survival of diverse B-cell malignancies, including chronic lymphocytic leukemia (CLL, involving naive B cells), mantle cell lymphoma (MCL) and marginal zone lymphoma (involving germinal center B cells), and Waldenström macroglobulinemia (WM, involving plasma cells). Consistent with a critical survival role for BTK in these malignancies, BTK deficiency abrogates tumor formation in CLL mouse models.[2] Treatment of primary, patient-derived CLL, MCL, and WM tumor cells with covalent (irreversible) BTK inhibitors (cBTKis) reduces viability, adhesion, and migration.[3-5]

The treatment landscape of B-cell malignancies has been transformed with cBTKi. Three cBTKis, ibrutinib, acalabrutinib, and zanubrutinib, are approved for MCL and CLL, whereas ibrutinib and zanubrutinib are also approved for WM and marginal zone lymphoma.[6-8] Despite advancing treatment, long-term efficacy with cBTKis has been limited by toxicity and acquired resistance.[9-12]

Pirtobrutinib, an orally available, highly selective, noncovalent (reversible) BTKi, with low-nanomolar potency against both BTK and BTK C481 substitution mutants, was developed to overcome multiple mechanisms of pharmacologic and on-target cBTKi resistance.[13] To deliver tonic inhibition throughout the dosing period, pirtobrutinib achieves exposures providing >90% inhibition of BTK at trough, regardless of the intrinsic BTK turnover rate. In a phase 1/2, multicenter, open-label clinical trial[14] with 725 patients treated across 7 dose levels, pirtobrutinib monotherapy was shown to be safe and have activity in

patients with multiple cBTKi-treated B-cell malignancies, including those with resistance in the absence of BTK C481 mutations.[15-18] The objective of this study was to provide a detailed preclinical characterization of pirtobrutinib.

Methods

Drugs

Pirtobrutinib was provided by Loxo@Lilly (Stamford, CT). Ibrutinib, acalabrutinib, and zanubrutinib were purchased from Selleck Chemicals (Houston, TX) and MedChemExpress (Monmouth Junction, NJ). Stock solutions were made in dimethyl sulfoxide (DMSO).

X-ray crystallography

GST-tagged, human BTK and BTK C481S kinase domain (residues 389-659) proteins were expressed in *Trichoplusia ni* insect cells. Purified proteins were crystallized in solution containing between 31% and 32% PEG3350, 0.3M ammonium sulfate, 0.1M bis-tris pH 5.5, with a single round of microseeding. Data collection, processing, and refinement statistics are summarized in supplemental Table 1 (available on the *Blood* website).[19-24] Pirtobrutinib omit electron density maps are shown in supplemental Figure 1.

Biochemical kinase assays

Pirtobrutinib activity against BTK, BTK C481S, and selected non-BTK kinases was determined by monitoring incorporation of [^{33}P]-PO_4 from [^{33}P]-adenosine triphosphate (ATP) into polyglutamic acid–tyrosine (poly-EY) peptide substrate in the HotSpot Kinase Assay (Reaction Biology, Malvern, PA).[25] Data were analyzed using standard-curve fitting methods. Pirtobrutinib (1 μM) was tested for kinase activity inhibition of 371 human kinases using the HotSpot Kinase Assay and K_m ATP concentrations. Pirtobrutinib, ibrutinib, zanubrutinib, and acalabrutinib (100 nM) were tested using the HotSpot Kinase Assay at a concentration of 10 μM ATP. Percentage of control activity was calculated for each enzyme.

Surface plasmon resonance

All experiments were performed with a Biacore T200 SPR system (Cytiva, Marlborough, MA) at 4°C in HBS-P running buffer (10 mM *N*-2-hydroxyethylpiperazine-*N*′-2-ethanesulfonic acid, pH 7.4; 150 mM NaCl; 10 mM $MgCl_2$; 2 mM Tris[2-carboxyethyl] phosphine; 0.05% [v/v] Tween 20; and 2% [v/v] DMSO). The full-length biotinylated BTK and BTK C481S proteins (Carna Biosciences, Kobe, Japan) were individually immobilized on a Series S streptavidin sensor chip at a density of ~5000 response units. The assay was performed using the Biacore single-cycle kinetics program with increasing pirtobrutinib concentrations passed over the sensor chip surface. Individual injection association and dissociation times were 120 seconds each, with a final dissociation event of 1800 seconds. Affinity constants were calculated with Biacore T200 evaluation software version 3.1.

Differential scanning fluorometry

N-terminal 6×-His–tagged BTK (1-659) and SH3-SH2-KD BTK (214-659) were expressed and purified at Loxo@Lilly. Proteins were assayed at 1 or 2 μM (BTK and SH3-SH2-BTK, respectively) with 100 μM BTKi and 2× SYPRO Orange dye in buffer containing 25 mM *N*-2-hydroxyethylpiperazine-*N*′-2-ethanesulfonic acid (pH 7.5), 10 mM $MgCl_2$, 0.5 mM Tris(2-carboxyethyl) phosphine, and 1% (v/v) DMSO. Assay plates were read on the QuantStudio 6 Pro quantitative polymerase chain reaction system using the Protein Thermal Shift protocol (20°C, 2 minutes; 0.05°C/s ramp; 95°C, 2 minutes).

Cell lines and cell cultures

TMD8 cells were obtained from Tokyo Medical and Dental University (Tokyo, Japan). HEK293T, HEK293, Ramos RA1, REC-1, HCT116, and A375 cells were obtained from the American Type Culture Collection (Manassas, VA). TMD8, REC-1, and Ramos RA1 cells were cultured in RPMI 1640 plus 10% fetal bovine serum (FBS). HEK293T, HEK293, and A375 cells were grown in Dulbecco's modified Eagle medium plus 10% FBS, and HCT116 cells were grown in McCoy's medium plus 10% FBS. TMD8 cells expressing BTK C481S were generated by electroporation of a BTK C481S plasmid and selection with 100 nM ibrutinib. This cell line also expresses endogenous BTK. HEK293T stably expressing BTK or BTK C481S were generated using standard transfection methods (GenScript Biotech, Piscataway, NJ). Whole blood was obtained from AllCells (Alameda, CA). Peripheral blood mononuclear cells (PBMCs) derived from patients with CLL were obtained from Discovery Life Sciences (Huntsville, AL), Precision for Medicine (Carlsbad, CA), and BioIVT (Hicksville, NY).

Cell proliferation assays

TMD8, TMD8 BTK C481S, and REC-1 cells were plated in 384-well plates at 1500 cells per well (TMD8) and 2500 cells per well (REC-1), and inhibitors at different concentrations were added to each well, in duplicate or triplicate. After a 72-hour incubation, cells were lysed with CellTiter-Glo reagent (Promega Corporation, Madison, WI). Luminescence was measured using the EnVision 2105 plate reader (PerkinElmer, Waltham, MA). Signals in compound-containing wells were normalized to signals from DMSO-containing wells and half-maximal inhibitory concentration (IC_{50}) values were calculated by using a 4-parameter fit.

Cellular phosphorylation assays

HEK293 cells stably expressing BTK or BTK C481S were plated in 96-well (1.5×10^5 cells per well) or 6-well plates (5×10^5 cells per well) and incubated with inhibitors for 2 hours. BTK Y223 autophosphorylation was assessed using Simple Western (ProteinSimple, San Jose, CA). For a full list of antibodies used see supplemental Table 2. The BTK Y223 phosphorylation signal was normalized to total BTK, and IC_{50} values were calculated relative to the percentage DMSO control, using a 4-parameter fit.

Ramos RA1 and REC-1 cells (8×10^6 cells per condition) were serum starved for 4 hours, incubated with pirtobrutinib for 2 hours, and then stimulated with anti-immunoglobulin M (anti-IgM) (5 μg/mL) for 10 minutes. PBMCs derived from donors with CLL (1.5×10^6 cells per condition) were incubated with pirtobrutinib for 3 hours. Cells were harvested, washed, and lysed, and then analyzed by Simple Western or traditional western blotting for levels of phosphorylated (phospho-) BTK Y223, phospho-BTK Y551, and total BTK. Phosphorylation signals were normalized to total BTK protein.

Activation of human PBMCs

Cryopreserved lymphocyte-enriched PBMCs isolated from whole blood were thawed and incubated overnight in RPMI 1640 with 10% FBS at 37°C. The next day, PBMCs were seeded in 96-well v-bottom plates at 2×10^5 cells per well and treated with pirtobrutinib for 1 hour. PBMCs were then stimulated with 10 μg/mL anti-IgM for 3 hours, washed, and incubated with anti-CD19-PE and CD69-APC antibodies and eFluor520 viability dye for 30 minutes at 4°C. The percentage of $CD69^+$ cells in the $CD19^+$ population was analyzed using FlowJo SW (BD Bioscience, Ashland, OR).

Calcium flux assay

REC-1 and TMD8 cells were plated in 96-well plates at 2×10^5 and 1×10^5 cells per well, respectively, in serum-free RPMI 1640. Cells were treated with pirtobrutinib for ~100 minutes followed by incubation with a Calbryte 520AM/Pluronic F-127 mixture at a 1:1 ratio for 30 minutes. Following incubation, cells were stimulated with anti-IgM to induce calcium flux and the fluorescent signal was read on an EnVision 2105 plate reader.

Other cellular activity assays

To quantify cellular target engagement of pirtobrutinib to BTK, BRK, TXK, YES1, CSK, FYN, and TEC, HEK293 cells were transiently transfected with full-length NanoLuc fusion vectors for each protein. Next, cells were incubated with a cell-permeable fluorescent NanoBRET tracer that reversibly binds to the kinase-NanoLuc luciferase fusion proteins. After incubation, cells were plated and treated with 3-fold serial dilutions of pirtobrutinib for 1 hour, followed by incubation with luciferase substrate (Promega Corporation, Madison, WI). Emission signals were measured with the EnVision 2104 plate reader and IC_{50} values were calculated using GraphPad Prism 4, based on a sigmoidal dose-response equation.

To quantify pirtobrutinib cellular activity against ERBB4, the PathHunter Functional Kinase assay was used (Eurofins/DiscoverX, St Charles, MO). U2OS cells (human bone osteosarcoma epithelial), engineered to coexpress the full-length receptor tyrosine kinase of interest and a tagged SH2 domain, were incubated with a range of pirtobrutinib concentrations. Pirtobrutinib IC_{50} values were determined using a 4-parameter fit.

To determine the cellular activity of pirtobrutinib for MEK1/MEK2, ERK1/ERK2 phosphorylation was evaluated in the HCT116 and A375 cell lines. Cells were plated at 5000 cells per well and treated with serially diluted pirtobrutinib. After 2 hours of treatment, cells were fixed, permeabilized, and incubated overnight with a phosphor-ERK1/2 (T202, Y204) primary antibody. A goat antirabbit IgG Alexa-488 secondary antibody was added, followed by fluorescence analysis with Acumen Explorer (SPT Labtech, Melbourn, United Kingdom) to count phospho-ERK1/2–positive cells. Data were analyzed using standard-curve fitting methods.

Tumor xenograft studies

OCI-Ly10 cells were implanted subcutaneously into male non-obese diabetic/severe combined immunodeficiency mice and tumors were allowed to grow to a volume of between ~150 and 200 mm^3. Mice were randomized by tumor size across dose groups and dosed orally twice-daily (BID) with 10 or 50 mg/kg pirtobrutinib (12 mice per group) or vehicle (11 mice per group) for 28 days. Tumor volumes were measured thrice weekly during the study and for an additional 35 days after dosing (Axis Bioservices, Coleraine, United Kingdom). In the TMD8 study, cells were injected subcutaneously into Balb/c SCID mice and allowed to grow for 19 days until a mean tumor volume of 400 mm^3 was reached. Mice were randomized by tumor size across dose groups and orally dosed BID with 15 or 30 mg/kg pirtobrutinib (10 mice per group) for 18 days or vehicle (10 mice per group) for 14 days. Tumor volumes were measured thrice weekly. REC-1 cells were injected subcutaneously into female athymic nude mice and allowed to grow for 18 days when a mean tumor volume of 150 mm^3 was reached. Mice were randomized by tumor volume across dose groups and orally dosed BID with pirtobrutinib at 10, 30, or 50 mg/kg (6 mice per group) or vehicle (10 mice per group) for 21 days. Tumor volumes were measured twice weekly. TMD8 cells expressing BTK C481S were injected into female Balb/c SCID mice and allowed to grow for 12 days when a mean tumor volume of 150 mm^3 was reached. Mice were randomized by tumor size and orally dosed BID with pirtobrutinib at 3, 10, and 30 mg/kg (10 mice per group) or vehicle (14 mice per group) for 14 days. Tumor volumes were measured 2 or 3 times per week.

Animal procedures for the OCI-Ly10 xenograft tumor studies were performed under the guidance of the United Kingdom Animal (Scientific Procedures) Act 1986. Mice used in the TMD8 and TMD8 BTK C481S studies were treated in accordance with guidelines by the Association for Assessment and Accreditation of Laboratory Animal Care International, and protocols were authorized by the French Ministry of Education, Advanced Studies and Research. All procedures used in the REC-1 xenograft study were compliant with the United States Department of Agriculture's Animal Welfare Act (9 CFR Parts 1, 2, and 3) and the Guide for the Care and Use of Laboratory Animals (Institute for Laboratory Animal Research, The National Academies Press, Washington, DC).

Statistical analysis

For the OCI-Ly10 and TMD8 BTK C481S in vivo xenograft studies, a 2-way, repeated-measures analysis of variance and Dunnett multiple comparison test were performed to compare tumor volume of each treatment group vs that in the vehicle control group. For TMD8 and REC-1 in vivo xenograft studies, a 2-way, repeated-measures analysis of variance was performed on log-transformed data to compare the tumor volume of each treatment group vs that in the vehicle control group. For the TMD8 study, analysis was performed until day 14 after randomization because no data were available for the vehicle group beyond this day. Differences with a P value $< .05$ were considered significant.

Percentage tumor growth inhibition (%TGI) was calculated as

$$\%TGI = [1 - (T - BL) / (C - BL)] \times 100,$$

in which T and C are mean end point tumor volumes in the treated and control groups, respectively. Baseline (BL) is the mean tumor volume for all groups at baseline (randomization) day. Percentage of tumor regression (%Reg) was calculated as

$$\%Reg = 100 \times (T - BL) / BL).$$

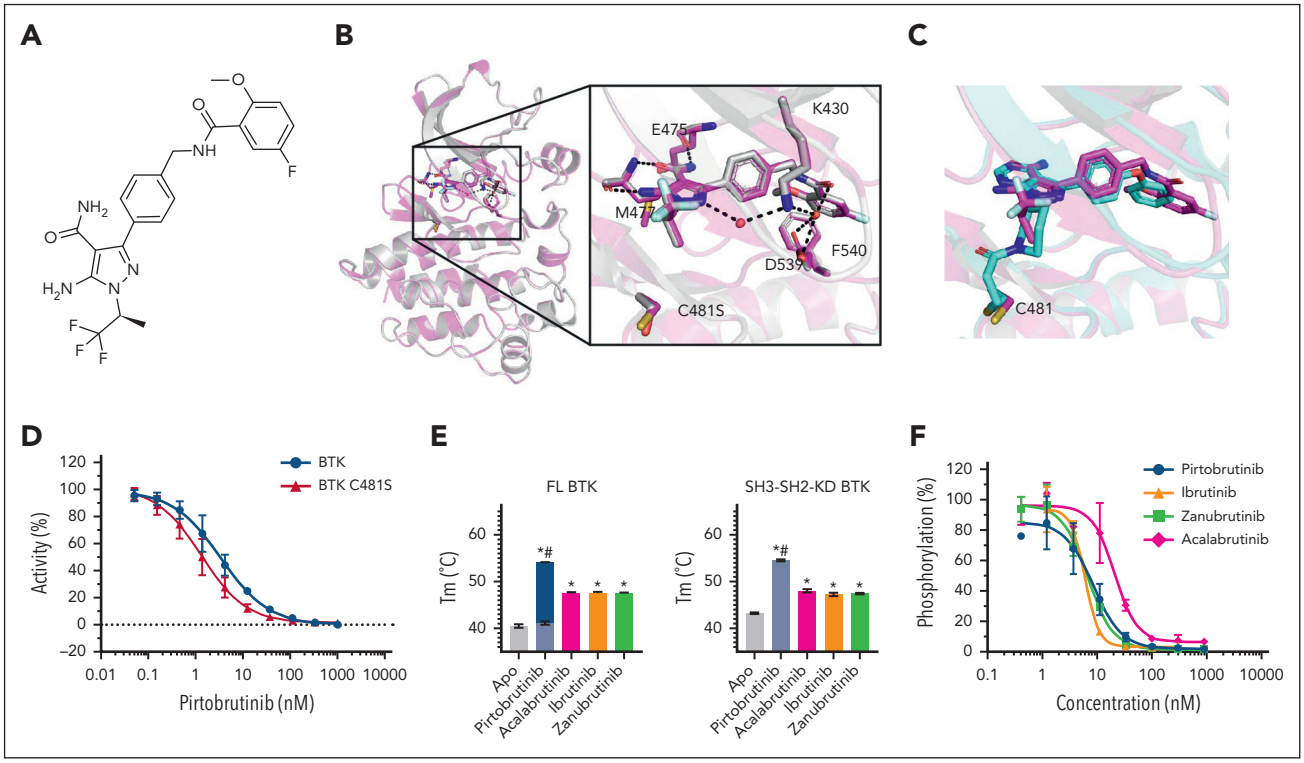

Figure 1. Pirtobrutinib structure, binding mode, and effects on BTK stability and activity. (A) Chemical structure of pirtobrutinib. (B) Superposition of the crystal structures of BTK and BTK C481S in complex with pirtobrutinib (magenta and light gray cartoon/stick representation, respectively; selected water molecules are shown as red spheres, and hydrogen bond interactions are illustrated as dashed lines). (C) BTK in complex with pirtobrutinib (magenta cartoon/stick representation) overlayed with BTK covalently bound to ibrutinib (cyan cartoon/stick representation; PDB ID 5P9J). (D) Dose-response curves showing inhibition of BTK and BTK C481S kinase activity by pirtobrutinib (n = 10) (mean and SD are graphed). (E) Tm graphs showing pirtobrutinib- and cBTKi-induced increases in full-length and SH3-SH2-KD BTK Tm. Light and dark blue bars represent the first and second pirtobrutinib-induced melting events, respectively; *P < .05 (compared with Apo Tm); #P < .05 (compared with each cBTKi's Tm). (F) Dose-response curves showing inhibition of cellular Y223 BTK phosphorylation in HEK293 cells stably expressing BTK by pirtobrutinib, ibrutinib, zanubrutinib, and acalabrutinib (n = 3) (mean and SD are graphed). FL, full-length; SD, standard deviation.

Results

X-ray crystal structures

X-ray crystal structures were generated for the kinase domain of BTK and BTK C481S in complex with pirtobrutinib (Figure 1A). The structures exhibited a global estimated root-mean-square deviation of ~0.7 Å and showed pirtobrutinib-bound in the ATP-binding site. The structural organization within the kinase domain was similar to previously published BTK x-ray crystal structures.[26-28] Pirtobrutinib formed 3 hydrogen bond interactions with the backbone of E475 and M477 in the hinge region, water-mediated hydrogen bonds with K430 and D539, and an edge-to-face pi-stacking interaction with F540 (Figure 1B). With a closest distance of ~4 Å, pirtobrutinib did not directly interact with C481 and introduction of the C481S mutation did not alter pirtobrutinib's binding interactions with BTK. In contrast, the United States Food and Drug Administration (FDA)-approved inhibitors ibrutinib,[27,28] zanubrutinib,[28] and acalabrutinib[28,29] are all irreversible and form a covalent bond with C481. The superimposed structures of pirtobrutinib with ibrutinib (Figure 1C) and zanubrutinib (supplemental Figure 2) showed that pirtobrutinib extends further into the BTK protein toward the activation loop and C-helix compared with ibrutinib and zanubrutinib.

Pirtobrutinib kinase inhibition and binding characterization

Pirtobrutinib demonstrated potent inhibition of BTK and BTK C481S in radiometric in vitro enzyme assays, with IC_{50} values of 3.2 and 1.4 nM, respectively (Figure 1D). SPR binding studies demonstrated pirtobrutinib is a reversible inhibitor of BTK and BTK C481S, with single-digit nanomolar binding affinities (K_D), low dissociation rates, and BTK and BTK C481S–pirtobrutinib complex half-lives ($t_{1/2}$) ranging from 1.5 to 2.4 hours (Table 1, supplemental Figure 3). In thermal melt studies using differential scanning fluorometry, pirtobrutinib binding to BTK resulted in 2 melt temperatures (Tms) of 41.2°C and 54.0°C, whereas the cBTKis each resulted in a single Tm of 47.5°C (mean value, Figure 1E). When all BTKis were subsequently evaluated against SH3-SH2-KD BTK (ΔPHTH-BTK), the Tms of truncated BTK bound to pirtobrutinib and cBTKis were 54.5°C and 47.5°C, respectively (Figure 1E). These data suggest that pirtobrutinib and cBTKi binding differentially stabilizes the PHTH and SH3-SH2-KD of BTK.

Inhibition of cellular BTK and BTK C481 activity

In HEK293 cells stably expressing BTK or BTK C481S, pirtobrutinib inhibited BTK Y223 autophosphorylation with IC_{50} values of 8.8 and 9.8 nM, respectively (Figure 1F; supplemental Figure 4). Although ibrutinib, acalabrutinib, and zanubrutinib also potently inhibited autophosphorylation in BTK-expressing cells, with IC_{50} values of 6.2, 20.8, and 6.6 nM, respectively, they showed minimal or no inhibitory activity in BTK C481S–expressing cells (supplemental Figure 4). Pirtobrutinib's potent inhibition of BTK autophosphorylation was maintained in HEK293T cells transiently expressing other BTK C481X mutants,

Table 1. Binding kinetics of pirtobrutinib with BTK and BTK C481 substitution mutants

Pirtobrutinib	Average k_{on}, $M^{-1}s^{-1}$	Average k_{off}, s^{-1}	Average K_D, nM	Average $t_{1/2}$, h	n
BTK	8.2 E+04	7.9 E−05	1.0	2.4	3
BTK C481S	8.5 E+04	1.3 E−04	1.5	1.5	3

K_D, dissociation equilibrium constant (nM) = k_{off}/k_{on}; k_{off}, dissociation rate constant (s^{-1}); k_{on}, association rate constant ($M^{-1}s^{-1}$); n, number of samples; $t_{1/2}$, complex half-life (hours) = ln $2/k_{off}$.

including C481T, C481G, and C481R, resulting in IC_{50} values ranging between 3.9 to 13.9 nM (supplemental Table 3). In Ramos RA1 and REC-1 cells, pirtobrutinib potently inhibited BTK phosphorylation of both Y223 (autophosphorylation) and Y551 (upstream kinase phosphorylation) (Figure 2A; supplemental Figure 5A). In contrast, although cBTKis potently inhibited Y223 phosphorylation in these cells, their effects on Y551 phosphorylation were minimal. In Ramos RA1, and REC-1 cells, pirtobrutinib also inhibited phosphorylation of the downstream substrate, PLCγ2 Y1217, with an IC_{50} of 9.1 nM and 51.7 nM, respectively (supplemental Figure 5B-C). In addition, in PBMCs from 4 treatment-naive donors with CLL, pirtobrutinib inhibited BTK Y223 autophosphorylation with an average IC_{50} of 2.3 nM (Figure 2B). Pirtobrutinib also potently inhibited Y551 phosphorylation in the 4 CLL samples, whereas ibrutinib had no effect (Figure 2C). Collectively, these findings confirm that pirtobrutinib inhibits BTK and BTK C481 mutant activity and suggest that pirtobrutinib binding compared with cBTKi binding differentially affects phosphorylation at Y551.

Inhibition of proliferation and downstream signaling in B-cell lines

Pirtobrutinib inhibited cell proliferation in TMD8 (Figure 3A) and REC-1 cells (supplemental Figure 6), with IC_{50} values of 6.4 and 3.1 nM, respectively, indicating potent cell proliferation inhibition in both activated B-cell diffuse large B-cell lymphoma (ABC-DLBCL) and MCL cell lines. Ibrutinib, acalabrutinib, and zanubrutinib also showed potent antiproliferative activities in TMD8 and REC-1 cells, with IC_{50} values ranging from 0.5 to 5.9 nM (Figure 3A; supplemental Figure 6). Although pirtobrutinib's antiproliferative potency was maintained in TMD8 cells expressing BTK C481S (IC_{50}, 26.4 nM), no antiproliferative activity was observed in these cells with cBTKis (Figure 3B).

Pirtobrutinib dose-dependently reduced anti-IgM–stimulated calcium flux, with IC_{50} values of 6.3 and 8.6 nM for TMD8 (Figure 3C) and REC-1 (Figure 3D), respectively. Ibrutinib, zanubrutinib, and acalabrutinib reduced anti-IgM–stimulated calcium flux in REC-1 cells, with IC_{50} values of 1.7 nM, 4.3 nM, and 72.7 nM, respectively (supplemental Figure 7). Pirtobrutinib treatment of REC-1 cells for 24 hours resulted in a >50% reduction of cytokine levels for 7 of 18 secreted cytokines detected in the untreated control, with IC_{50} values ranging from 2.6 to 6.1 nM (supplemental Table 4). In healthy-donor human PBMCs, pirtobrutinib reduced the anti-IgM–induced CD69 expression on $CD19^+$ B cells in a dose-dependent manner (IC_{50}, 4.7 ± 1.7 nM) (Figure 3E-F). In addition, in T cells isolated from healthy donors, pirtobrutinib did not affect the proliferation, viability, cell size, and expression of PD-1, TIM3, and LAG3 in a T-cell activation/exhaustion in vitro assay (supplemental Figure 8). Ibrutinib treatment showed similar results (supplemental Figure 8). Collectively, results indicate that pirtobrutinib potently inhibited proliferation, anti-IgM–stimulated calcium flux and CD69 expression, and cytokine secretion in B cells.

Inhibition of ABC-DLBCL and MCL xenograft tumor growth

In vivo pirtobrutinib efficacy was evaluated in mouse xenograft models using human ABC-DLBCL cell lines (OCI-Ly10 and TMD8), and the MCL cell line, REC-1. The pharmacokinetic profile in mice (supplemental Figure 9) differs from that in humans and requires BID oral dosing to maintain exposure throughout the dosing period. Pirtobrutinib caused significant dose-dependent TGI in the 3 xenograft models. In the OCI-Ly10 model, TGI was 88% and 95% at 10 and 50 mg/kg BID, respectively, on treatment day 28 (Figure 4A). Only modest tumor regrowth was observed after pirtobrutinib withdrawal for 35 days, with 83% and 93% TGI maintained in the 10 and 50 mg/kg treatment groups, respectively (Figure 4A). In the TMD8 xenograft model, a dose-dependent 76% and 101% TGI at 15 and 30 mg/kg BID, respectively, on treatment day 14, was observed with pirtobrutinib compared with vehicle (Figure 4B). Tumor regression (TR) of –49% was observed in the 30 mg/kg BID group on treatment day 18, when compared with tumor volumes at treatment initiation. In the REC-1 MCL xenograft model, pirtobrutinib demonstrated 80% and 84% TGI at 10 and 30 mg/kg BID, respectively, and TR of –11% in the 50 mg/kg BID group (Figure 4C). In vivo pirtobrutinib efficacy was also evaluated in a human DLBCL TMD8 BTK C481S xenograft model (Figure 4D). A significant dose-dependent TGI at 10 and 30 mg/kg BID was observed with pirtobrutinib treatment compared with vehicle-treated control. TR of –29% and –48% were observed at 10 and 30 mg/kg BID, respectively, compared with tumor volumes at treatment initiation. All treatments were well tolerated, and no drug-related deaths occurred in the 4 lymphoma xenograft studies (supplemental Figure 10).

Biochemical and cellular assays

Pirtobrutinib was profiled against 371 kinases in enzyme activity assays at a 1 μM concentration (supplemental Table 5). Results show only BTK and 8 other kinases were inhibited by >50% at 1 μM. Follow-up dose-response assays showed pirtobrutinib inhibited 6 kinases with <100-fold selectivity vs BTK (supplemental Table 6). To compare kinase selectivity across BTK inhibitors, pirtobrutinib, ibrutinib, zanubrutinib, and acalabrutinib were profiled against 371 (pirtobrutinib and ibrutinib), 367 (zanubrutinib), and 362 (acalabrutinib) kinases at 100 nM (supplemental Table 5). Pirtobrutinib showed improved selectivity with only 4 kinases inhibited >50% compared with ibrutinib and zanubrutinib, which inhibited 22 and 6 kinases,

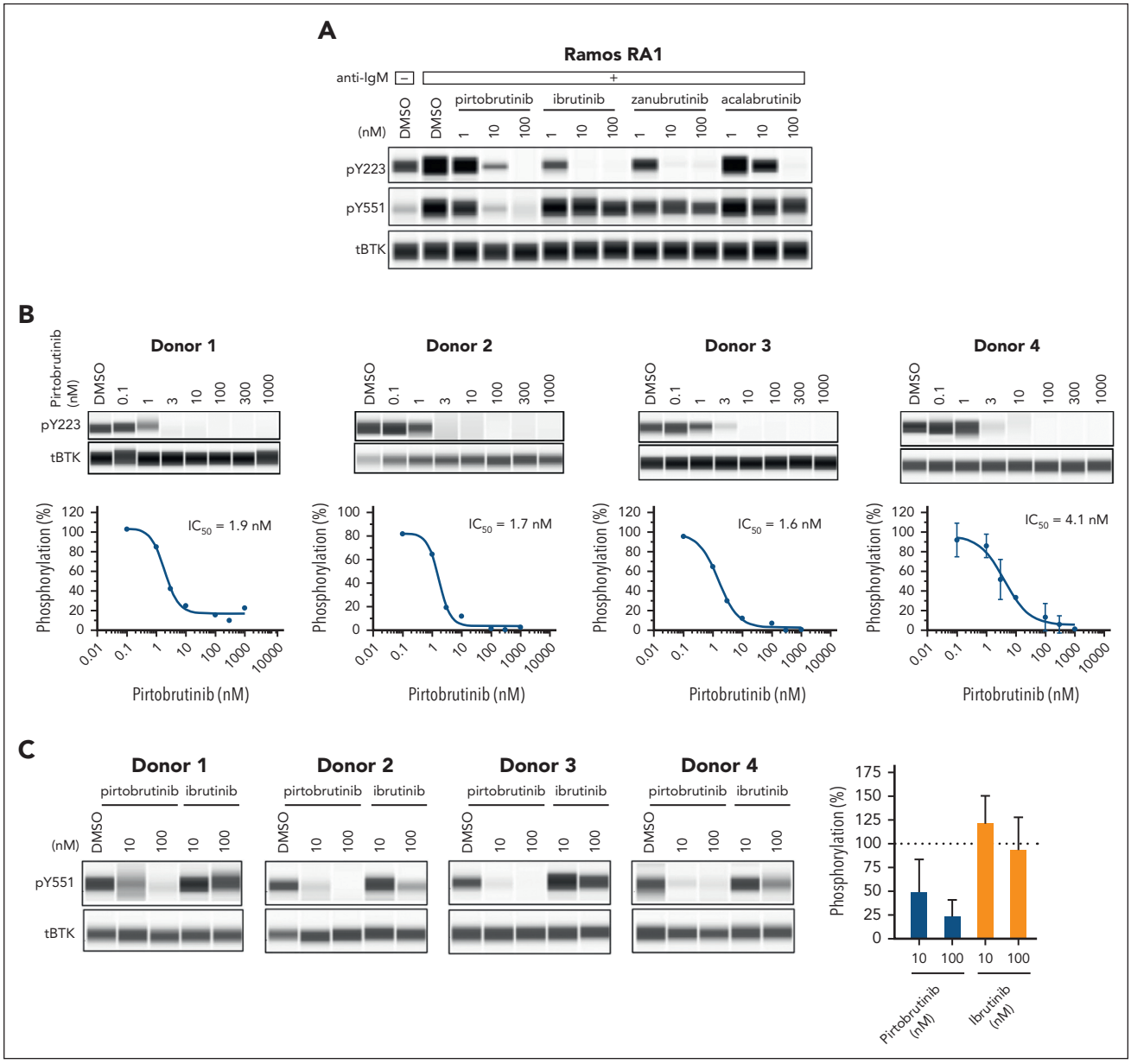

Figure 2. Differential impact of pirtobrutinib and cBTKis on BTK phosphorylation in Ramos RA1 cells and human CLL cells. Autophosphorylation at BTK Y223 and phosphorylation at BTK Y551 were measured by Simple Western in Ramos RA1 cells (A) and human CLL cells (B and C). (A) Ramos RA1 cells were treated with pirtobrutinib, ibrutinib, acalabrutinib, or zanubrutinib for 2 hours before stimulation with anti-IgM for 10 minutes. A representative Simple Western image shows the differential effect of pirtobrutinib vs the cBTKis on BTK Y551 phosphorylation in these cells. (B) PBMCs from 4 treatment-naive donors with CLL were treated with ascending doses of pirtobrutinib. Simple Western images show the potent inhibition of pirtobrutinib on BTK Y223 phosphorylation, with corresponding dose-response curves and calculated IC_{50} values shown below. Donor 4 was tested in 2 independent experiments with mean ± SD shown. (C) PBMCs from the 4 donors with CLL were treated with pirtobrutinib or ibrutinib at 10 or 100 nM. Simple Western images and a corresponding bar chart show the differential effect of pirtobrutinib and ibrutinib on Y551 phosphorylation in the PBMCs from the 4 donors with CLL (mean and SD are graphed). DMSO is measured in percentage for all blots. pY223, phospho-BTK Y223; pY551, phospho-BTK Y551; tBTK, total BTK.

respectively. In this assay, acalabrutinib inhibited 4 kinases, similar to pirtobrutinib, but was much less potent on BTK with only 83% inhibition, compared with the 97% inhibition observed for pirtobrutinib. To profile pirtobrutinib's cellular selectivity, a competitive binding chemoproteomics study was performed in which PBMCs were incubated with or without pirtobrutinib (10, 1, 0.1, and 0.01 μM), before incubation with biotinylated acyl phosphates, ATP and adenosine diphosphate, which react irreversibly with conserved lysine residues in the ATP-binding pockets of protein kinases. Mass spectrometry analysis showed, at 0.1 μM pirtobrutinib, probe binding to BTK was reduced by 90%, with no other kinase showing >50% reduction. At higher concentrations, besides BTK, only 3 other kinases showed >50% inhibition, TEC and MEK1/MEK2, at 1 and 10 μM pirtobrutinib, respectively (supplemental Table 7). In additional cell-based assays to characterize pirtobrutinib inhibition for select kinases of interest, pirtobrutinib retained >100-fold selectivity vs TEC, and was 500-fold selective for BTK over the other targets (Table 2).

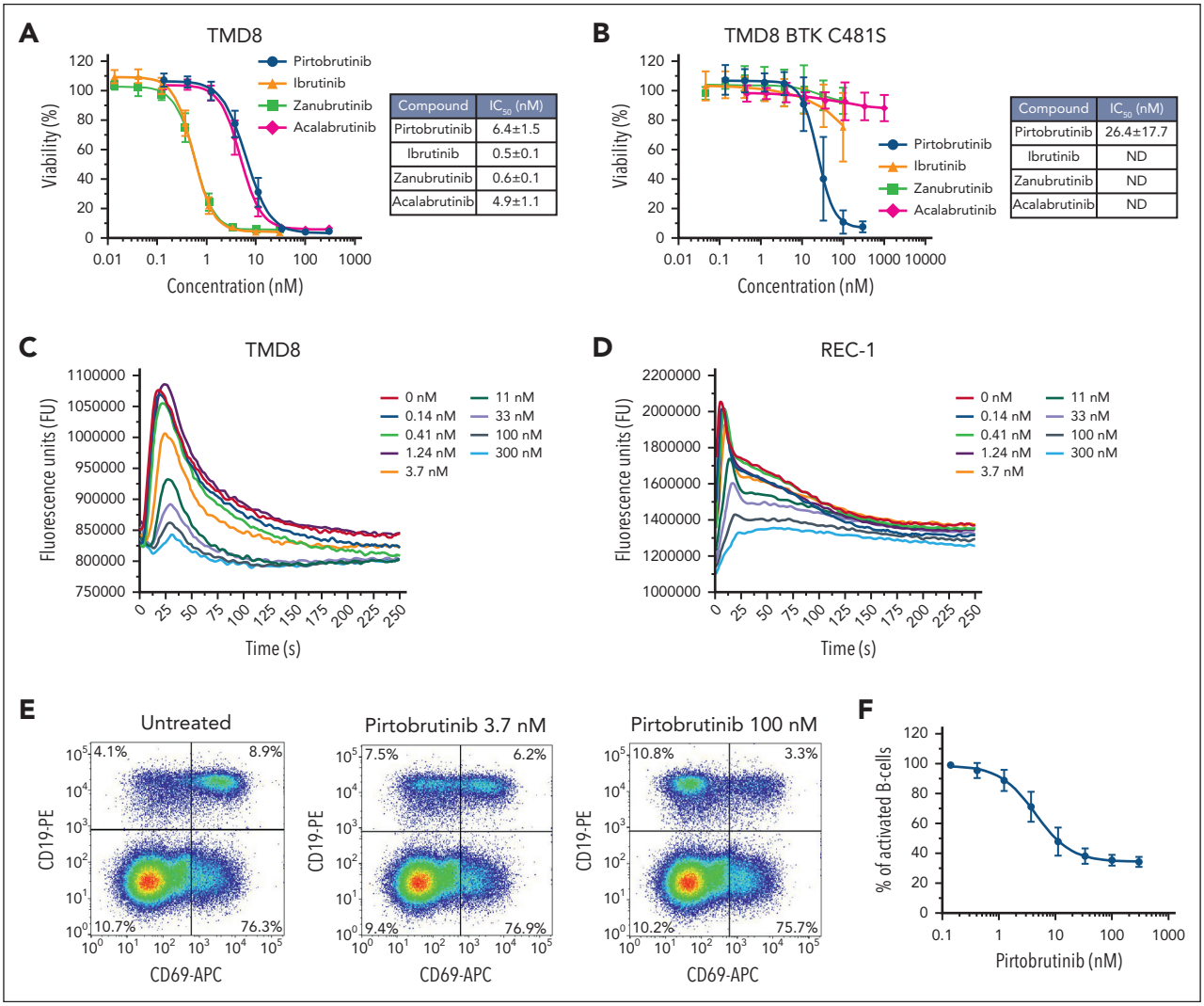

Figure 3. Pirtobrutinib inhibits cellular proliferation, B-cell activation, and calcium mobilization. (A) Activity of pirtobrutinib, ibrutinib, acalabrutinib, and zanubrutinib on cellular proliferation of TMD8 cells and (B) TMD8 cells expressing BTK C481S (mean and SD are graphed). (C) Pirtobrutinib inhibited anti-IgM–stimulated calcium flux in TMD8 and (D) REC-1 cells. Representative traces of 3 independent experiments are shown. (E) Human PBMCs from healthy donors were treated with pirtobrutinib, and B-cell activation was measured by upregulation of the CD69 activation marker after IgM stimulation. Representative flow cytometry density plots showing a reduction in the percentage of $CD19^+$ B cells expressing CD69 with increasing doses of pirtobrutinib. (F) Dose-response curve of pirtobrutinib inhibition of B-cell activation in PBMCs from 4 separate healthy donors. Data are mean ± SD.

Discussion

From the preclinical profile presented here, pirtobrutinib was shown to be a highly selective and a potent noncovalent BTKi. Pirtobrutinib inhibited both BTK and BTK C481 mutant variants with low-nanomolar potency. Furthermore, in vitro binding experiments demonstrated that pirtobrutinib dissociates slowly from BTK, and the pirtobrutinib-BTK complex half-life exceeded the reported mean half-lives of FDA-approved kinase inhibitors on their main target.[30] X-ray crystallography studies using the BTK kinase domain revealed that pirtobrutinib did not directly interact with C481 but displayed extensive hydrogen bonding with other BTK residues and water molecules in, or close to, the ATP-binding site, which are identical in both BTK and BTK C481S. Consequently, introduction of the C481S mutation did not alter pirtobrutinib's binding interactions with BTK. In contrast, acalabrutinib, ibrutinib, and zanubrutinib each form a covalent bond with C481.[27-29] Thus, whereas these cBTKis were shown to be largely inactive against C481 mutant forms of BTK in our studies, pirtobrutinib retained activity on C481 mutations. This is an important development in the treatment landscape for BTKis as the C481–binding site mutation appears to be the most common on-target resistance mechanism in CLL.[31,32] Other studies have shown C481 substitution mutations are a recurring mechanism of resistance to cBTKis, seen in varying rates across disease types.[31,33] C481 substitutions prevent irreversible ligation of cBTKis to BTK, leading to insufficient BTK target coverage in patients and treatment failure.[32,34] Second-generation cBTKis provide greater selectivity and limit off-target toxicity but efficacy after progression on cBTKis is limited because they do not overcome mechanisms of resistance.[12,35] Recently, BTK mutations other than C481, located in, and near, the ATP-binding site were identified in 7 patients treated with pirtobrutinib, who had previously received ibrutinib treatment.[12] The crystal structure of BTK bound to pirtobrutinib shows that these mutations are predicted to sterically block the binding of pirtobrutinib to the

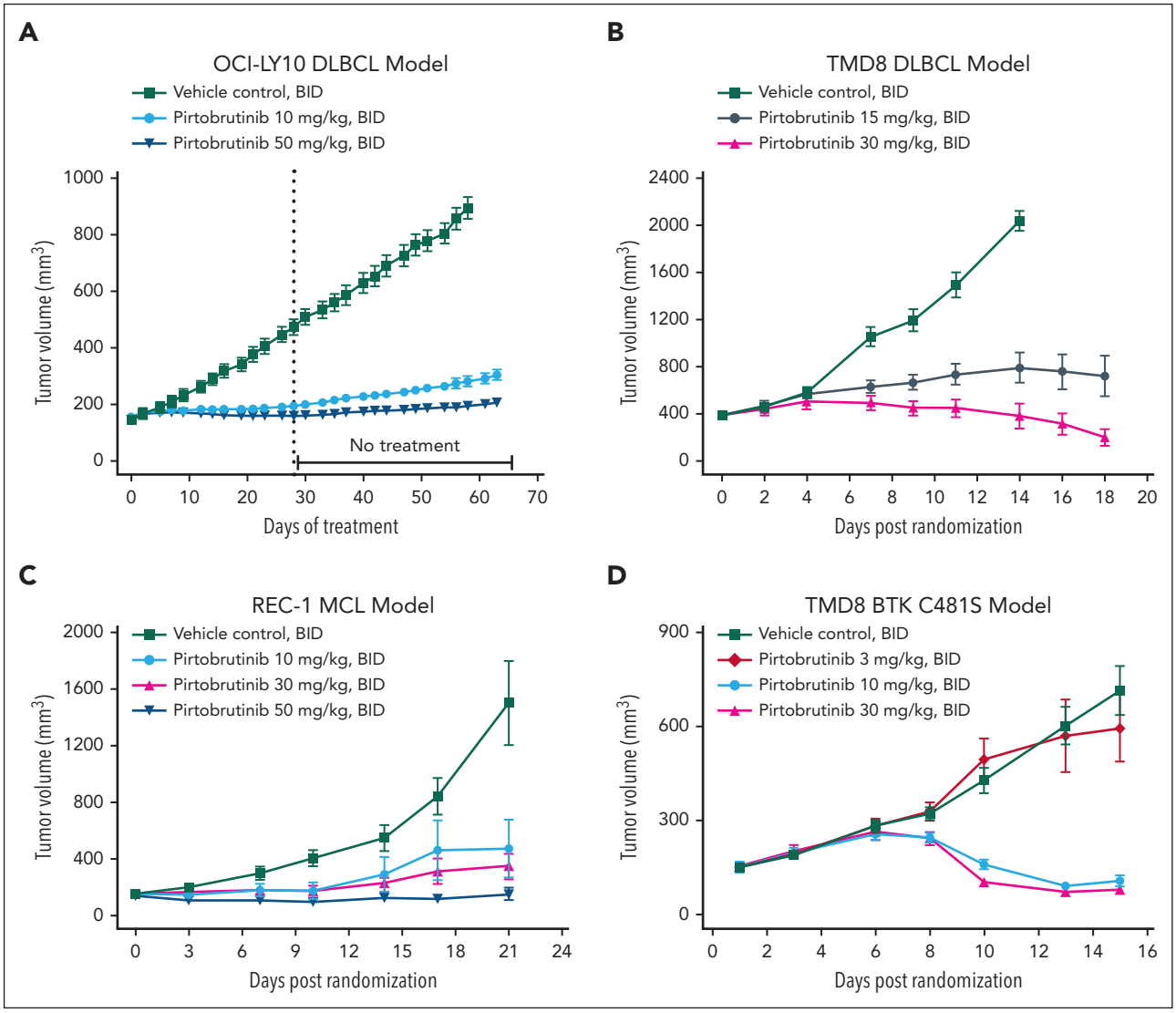

Figure 4. In vivo efficacy of pirtobrutinib in BTK and BTK C481S mutant lymphoma xenograft models. Tumor-bearing mice were treated with pirtobrutinib with the indicated doses, for the indicated time. Means and standard error of the mean were plotted for each treatment group vs days of treatment (A) or days after randomization (B-D). For OCI-LY10 xenografts (A), tumor volumes were measured 3 times per week, and the tumor volumes were measured for an additional 35 days after the last dose. For TMD8 xenografts (B), tumor volumes were measured 3 times per week. The experiment was stopped on day 14 after randomization for the vehicle control group, and on day 18 after randomization for the other groups. For REC-1 xenografts (C), tumor volumes were measured biweekly. For TMD8 BTK C481S xenografts (D), tumor volumes were measured 2 or 3 times per week.

protein. To date, these mutations have not been observed in patients treated with pirtobrutinib, who are naive to covalent inhibitor treatment. Additional studies to further explore pirtobrutinib resistance mechanisms are in progress. In addition, in patients, second-generation approved cBTKis have circulating half-lives ranging from 1 to 4 hours,[7,8] resulting in short exposure periods for binding to, and inactivation of, BTK.[6,7] Conversely, 200 mg pirtobrutinib daily has a circulating half-life of ~20 hours in patients with trough steady state exposure corresponding to 96% BTK target inhibition.[14] Pirtobrutinib's BTK inhibition at trough may be particularly important in patients with rapid BTK synthesis rates and in more proliferative tumors with high de novo BTK turnover, in which cBTKis may be limited by incomplete covalent target occupancy toward the end of the dosing interval, potentially driving disease progression and drug resistance.[14,36,37]

High pirtobrutinib selectivity for BTK was demonstrated in both enzymatic and cell-based systems. The x-ray crystal structure showed, in addition to numerous van der Waals and direct hydrogen bond interactions between pirtobrutinib and BTK, that pirtobrutinib interacts with the BTK protein through an extensive water-mediated hydrogen bond network. We hypothesize that the large number of pirtobrutinib interactions with BTK plays a role in pirtobrutinib's high kinome selectivity. Covalent BTKi off-target inhibition has been associated with toxicities,[10,11] such as antiplatelet bleeding activity associated with TEC inhibition.[38] Clinically, pirtobrutinib selectivity has translated into low toxicity across multiple B-cell malignancies, in which it demonstrated early promising safety, with low overall rates of adverse events and few discontinuations because of adverse events, including among patients intolerant to existing drugs.[14]

Table 2. Selectivity of pirtobrutinib in cell-based assays

Kinase	n	Pirtobrutinib IC_{50}, mean ± SD, nM	Fold selectivity vs BTK*	Cell assay readout
BTK	3	0.66 ± 0.34	1	Competitive displacement of tracer
TEC	3	70.46 ± 20.30	106.8	Competitive displacement of tracer
BRK/PTK6	3	360.47 ± 198.56	546.2	Competitive displacement of tracer
TXK	3	>5000†	>7600	Competitive displacement of tracer
YES1	3	>5000†	>7600	Competitive displacement of tracer
CSK	3	>5000†	>7600	Competitive displacement of tracer
FYN	3	>5000†	>7600	Competitive displacement of tracer
ERBB4	2	>10 000†	N/D	Phosphorylation of C-terminal tail
MEK1/MEK2	3	12 600 ± 2400	N/D	Phosphorylation of ERK1/2 (HCT116 cells)
MEK1/MEK2	3	3790 ± 1310	N/D	Phosphorylation of ERK1/2 (A375 cells)

N/D, not determined; n, number of samples; SD, standard deviation.

*Fold selectivity values vs BTK were calculated for those kinases assayed in the NanoBRET competitive displacement assay.

†When data values did not fit an IC_{50} curve, the top dose tested was used for estimating mean.

Experiments described herein demonstrated that pirtobrutinib inhibits BTK cellular activity and tumor growth in vivo across multiple tumor types. Pirtobrutinib inhibited BTK signaling and cell proliferation in multiple B-cell lymphoma cell lines, including DLBCL and MCL, and in PBMCs from treatment-naive donors with CLL, demonstrating in vitro activity in clinically relevant cell populations. In vivo results from mouse xenograft studies demonstrated that pirtobrutinib significantly inhibited tumor growth from human ABC-DLBCL and MCL lines and was well-tolerated in mice.

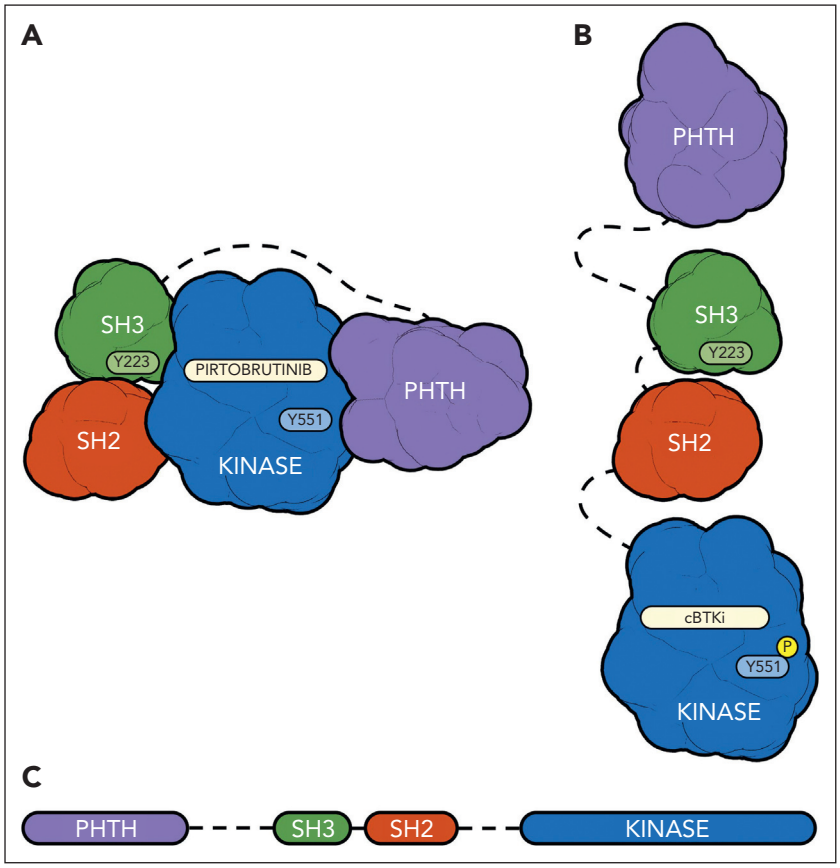

Figure 5. Hypothesized binding models for pirtobrutinib and covalent BTK inhibitor. (A) We hypothesize that pirtobrutinib stabilizes BTK in a closed, inactive conformation, whereas (B) cBTKi binding destabilizes the closed conformation, providing upstream kinase access to phosphorylate Y551. (C) A cartoon representation showing the domain organization of BTK.

Pirtobrutinib, but not cBTKis, prevented Y551 phosphorylation in the BTK activation loop in multiple cell assays. These results were unexpected because pirtobrutinib does not bind in the H3 selectivity pocket as previously described for other BTK inhibitors that prevent Y551 phosphorylation (supplemental Figure 11).[27] We also observed that pirtobrutinib maintained BTK in a folded state at a significantly higher temperature than apo- and cBTKi-bound BTK, as indicated by the increased Tm to 54.0°C of pirtobrutinib-bound full-length BTK, which is 13.5°C and 6.5°C more than apo- and cBTKi-bound BTK, respectively. We hypothesize that pirtobrutinib stabilizes BTK in a closed, inactive conformation, consistent with the high BTK-pirtobrutinib complex Tm, whereas cBTKis[39] destabilize the closed conformation, providing access to upstream kinases, which phosphorylate Y551 (Figure 5) and downstream scaffolding interactions. The closed, inactive conformation of BTK stabilized by pirtobrutinib binding may interact with fewer cellular proteins than cBTKi-bound BTK, thereby inhibiting kinase-independent BTK cellular signaling. Studies to characterize the functional differences between the pirtobrutinib-induced closed BTK conformation and the cBTKi-induced open BTK conformation are ongoing with a focus on identifying interactions with phosphorylated Y551, recently described with HCK,[40] and differentially exposed regions of BTK.

In conclusion, the pharmacologic, biophysical, and structural attributes detailed herein differentiated pirtobrutinib from the current FDA-approved cBTKis. In combination with the phase 1 and 2 clinical experience in multiple B-cell malignancies,[14] these results support the advancement of pirtobrutinib into ongoing phase 3 trials in MCL and CLL.

Acknowledgments

The authors thank Faith Watson, Omar Mendoza, Regina Choy, Jacob Shrier, Carmen Baquero, Maria Jose Lallena Jimeno, Wayne Blosser, and Karen Berg for their contributions to experiments and/or review of the manuscript.

This work was supported by Loxo@Lilly. This research used resources of the Advanced Photon Source; a US Department of Energy (DOE) Office of Science User Facility operated for the DOE Office of Science by Argonne National Laboratory under contract number DE-AC02-06CH11357. Use of the Lilly Research Laboratories Collaborative Access Team (LRL-CAT) beamline at Sector 31 of the Advanced Photon Source was provided by Eli Lilly and Company, which operates the facility. The funders provided support in the form of salaries for all authors. Andrea Metti provided medical writing support and Preethi Govindarajan and Dana Schamberger provided editorial support, which was funded by Eli Lilly and Company.

Authorship

Contribution: E.B.G., K.E., H.S.R., M.S.R., E.P.C., T.H.M., L.M.H., N.E.B., X.G., W.W., K.S.K., J.A.B., C.K.A., and B.J.B. designed research/experiments; E.B.G., H.S.R., M.S.R., T.H.M., L.M.H., N.E.B., J.S., W.W., I.L., and K.S.K. performed research/experiments; E.B.G., K.E., H.S.R., M.S.R., E.P.C., L.M.H., N.E.B., W.W., I.L., K.S.K., J.A.B., C.K.A., and B.J.B. analyzed the data; E.B.G., K.E., H.S.R., M.S.R., E.P.C., T.H.M., L.M.H., N.E.B., X.G., J.S., W.W., I.L., K.S.K., R.A.W., P.B.A., J.A.B., C.K.A., and B.J.B. participated in manuscript drafting and critical revisions of manuscript; and R.A.W., P.B.A., and B.J.B. supervised the project.

Conflict-of-interest disclosure: E.B.G., K.E., H.S.R., M.S.R., E.P.C., T.H.M., L.M.H., N.E.B., X.G., J.S., W.W., R.A.W., P.B.A., J.A.B., C.K.A., and B.J.B. are employees of Loxo@Lilly and minor shareholders (restricted stock units) of Eli Lilly and Company. I.L. and K.S.K. are former employees of Loxo@Lilly. K.S.K. reports being a minor shareholder (restricted stock units) of Eli Lilly and Company. B.J.B. reports having patent applications filed related to employment with Loxo@Lilly.

Correspondence: Kevin Ebata, Loxo@Lilly, 201 Haskins Way, Ste 400, South San Francisco, CA, 94080; email: kevin@loxooncology.com.

Footnotes

Submitted 22 December 2022; accepted 31 January 2023; prepublished online on *Blood* First Edition 16 February 2023. https://doi.org/10.1182/blood.2022018674.

*E.B.G. and K.E. contributed equally to the study.

Atomic coordinates and structure factors for the crystal structures of BTK and BTK C481S kinase domain in complex with pirtobrutinib were deposited in the Protein Data Bank with accession codes 8FLL and 8FLN, respectively. Additional data associated with this study are available in the article or the Supplementary Materials.

The online version of this article contains a data supplement.

The publication costs of this article were defrayed in part by page charge payment. Therefore, and solely to indicate this fact, this article is hereby marked "advertisement" in accordance with 18 USC section 1734.

REFERENCES

1. Rawlings DJ, Scharenberg AM, Park H, et al. Activation of BTK by a phosphorylation mechanism initiated by SRC family kinases. *Science*. 1996;271(5250):822-825.
2. Kil LP, de Bruijn MJ, van Hulst JA, Langerak AW, Yuvaraj S, Hendriks RW. Bruton's tyrosine kinase mediated signaling enhances leukemogenesis in a mouse model for chronic lymphocytic leukemia. *Am J Blood Res*. 2013;3(1):71-83.
3. Herman SEM, Gordon AL, Hertlein E, et al. Bruton tyrosine kinase represents a promising therapeutic target for treatment of chronic lymphocytic leukemia and is effectively targeted by PCI-32765. *Blood*. 2011;117(23):6287-6296.
4. Chang BY, Francesco M, De Rooij MFM, et al. Egress of CD19(+)CD5(+) cells into peripheral blood following treatment with the Bruton tyrosine kinase inhibitor ibrutinib in mantle cell lymphoma patients. *Blood*. 2013;122(14):2412-2424.
5. Yang G, Zhou Y, Liu X, et al. A mutation in MYD88 (L265P) supports the survival of lymphoplasmacytic cells by activation of Bruton tyrosine kinase in Waldenstrom macroglobulinemia. *Blood*. 2013;122(7):1222-1232.
6. Imbruvica prescribing information. Accessed 25 November 2022. https://www.imbruvica.com/files/prescribing-information.pdf
7. Calquence prescribing information. Accessed 25 November 2022. https://den8dhaj6zs0e.cloudfront.net/50fd68b9-106b-4550-b5d0-12b045f8b184/e2a005a7-65a0-4388-a671-dc887815a938/e2a005a7-65a0-4388-a671-dc887815a938_viewable_rendition__v.pdfhttps://den8dhaj6zs0e.cloudfront.net/
8. Brukinsa prescribing information. Accessed 25 November 2022. https://www.brukinsa.com/prescribing-information.pdf
9. Jensen JL, Mato AR, Pena C, Roeker LE, Coombs CC. The potential of pirtobrutinib in multiple B-cell malignancies. *Ther Adv Hematol*. 2022;13:20406207221101697.
10. Lipsky A, Lamanna N. Managing toxicities of Bruton tyrosine kinase inhibitors. *Hematology Am Soc Hematol Educ Program*. 2020;2020(1):336-345.
11. Patel V, Balakrishnan K, Bibikova E, et al. Comparison of acalabrutinib, a selective Bruton tyrosine kinase inhibitor, with ibrutinib in chronic lymphocytic leukemia cells. *Clin Cancer Res*. 2017;23(14):3734-3743.
12. Wang E, Mi X, Thompson MC, et al. Mechanisms of resistance to noncovalent

Bruton's tyrosine kinase inhibitors. *N Engl J Med*. 2022;386(8):735-743.

13. Brandhuber B, Gomez E, Smith S, et al. LOXO-305, a next generation reversible BTK inhibitor, for overcoming acquired resistance to irreversible BTK inhibitors. *Clin Lymphoma Myeloma Leuk*. 2018;18:S216.
14. Mato AR, Shah NN, Jurczak W, et al. Pirtobrutinib in relapsed or refractory B-cell malignancies (BRUIN): a phase 1/2 study. *Lancet*. 2021;397(10277):892-901.
15. Palomba ML, Patel MR, Eyre TA, et al. Efficacy of pirtobrutinib, a highly selective, non-covalent (reversible) BTK inhibitor in relapsed/refractory Waldenström macroglobulinemia: results from the phase 1/2 BRUIN study. *Blood*. 2022; 140(Supplement 1):557-560.
16. Wierda WG, Lewis DJ, Ghia P, et al. Efficacy of pirtobrutinib, a highly selective, non-covalent (reversible) BTK inhibitor in Richter transformation: results from the phase 1/2 BRUIN study. *Blood*. 2022;140(Supplement 1):846-849.
17. Wang ML, Shah NN, Jurczak W, et al. Efficacy of pirtobrutinib in covalent BTK-inhibitor pre-treated relapsed/refractory mantle cell lymphoma: additional patients and extended follow-up from the phase 1/2 BRUIN study. *Blood*. 2022;140(Supplement 1):9368-9372.
18. Mato AR, Woyach JA, Brown JR, et al. Efficacy of pirtobrutinib in covalent BTK-inhibitor pre-treated relapsed/refractory CLL/SLL: additional patients and extended follow-up from the phase 1/2 BRUIN study. *Blood*. 2022;140(Supplement 1):2316-2320.
19. Vonrhein C, Flensburg C, Keller P, et al. Data processing and analysis with the autoPROC toolbox. *Acta Crystallogr D Biol Crystallogr*. 2011;67(Pt 4):293-302.
20. Tickle IJ, Flensburg C, Keller P, et al. *STARANISO*. Global Phasing Ltd; 2018.
21. Bricogne G, Blanc E, Brandl M, et al. *BUSTER version 2.11.5*. Global Phasing, Ltd; 2017.
22. McCoy AJ, Grosse-Kunstleve RW, Adams PD, Winn MD, Storoni LC, Read RJ. Phaser crystallographic software. *J Appl Crystallogr*. 2007;40(Pt 4):658-674.
23. Emsley P, Lohkamp B, Scott WG, Cowtan K. Features and development of Coot. *Acta Crystallogr D Biol Crystallogr*. 2010;66(Pt 4): 486-501.
24. Smart OS, Womack TO, Sharff A, et al. *Grade, version 1.2.20*. Global Phasing Ltd; 2011. https://www.globalphasing.com
25. Anastassiadis T, Deacon SW, Devarajan K, Ma H, Peterson JR. Comprehensive assay of kinase catalytic activity reveals features of kinase inhibitor selectivity. *Nat Biotechnol*. 2011;29(11):1039-1045.
26. Mao C, Zhou M, Uckun FM. Crystal structure of Bruton's tyrosine kinase domain suggests a novel pathway for activation and provides insights into the molecular basis of X-linked agammaglobulinemia. *J Biol Chem*. 2001; 276(44):41435-41443.
27. Bender AT, Gardberg A, Pereira A, et al. Ability of Bruton's tyrosine kinase inhibitors to sequester Y551 and prevent phosphorylation determines potency for inhibition of Fc receptor but not B-cell receptor signaling. *Mol Pharmacol*. 2017;91(3):208-219.
28. Guo Y, Liu Y, Hu N, et al. Discovery of zanubrutinib (BGB-3111), a novel, potent, and selective covalent inhibitor of Bruton's tyrosine kinase. *J Med Chem*. 2019;62(17): 7923-7940.
29. Estupiñán HY, Wang Q, Berglöf A, et al. BTK gatekeeper residue variation combined with cysteine 481 substitution causes super-resistance to irreversible inhibitors acalabrutinib, ibrutinib and zanubrutinib. *Leukemia*. 2021;35(5):1317-1329.
30. Georgi V, Schiele F, Berger BT, et al. Binding kinetics survey of the drugged kinome. *J Am Chem Soc*. 2018;140(46):15774-15782.
31. Chiron D, Di Liberto M, Martin P, et al. Cell-cycle reprogramming for PI3K inhibition overrides a relapse-specific C481S BTK mutation revealed by longitudinal functional genomics in mantle cell lymphoma. *Cancer Discov*. 2014;4(9):1022-1035.
32. Woyach JA, Ruppert AS, Guinn D, et al. BTK(C481S)-mediated resistance to ibrutinib in chronic lymphocytic leukemia. *J Clin Oncol*. 2017;35(13):1437-1443.
33. Xu L, Tsakmaklis N, Yang G, et al. Acquired mutations associated with ibrutinib resistance in Waldenstrom macroglobulinemia. *Blood*. 2017;129(18):2519-2525.
34. Byrd JC, Furman RR, Coutre SE, et al. Targeting BTK with ibrutinib in relapsed chronic lymphocytic leukemia. *N Engl J Med*. 2013;369(1):32-42.
35. Bond DA, Woyach JA. Targeting BTK in CLL: beyond ibrutinib. *Curr Hematol Malig Rep*. 2019;14(3):197-205.
36. Gu D, Tang H, Wu J, Li J, Miao Y. Targeting Bruton tyrosine kinase using non-covalent inhibitors in B cell malignancies. *J Hematol Oncol*. 2021;14(1):40.
37. Alsadhan A, Cheung J, Gulrajani M, et al. Pharmacodynamic analysis of BTK inhibition in patients with chronic lymphocytic leukemia treated with acalabrutinib. *Clin Cancer Res*. 2020;26(12):2800-2809.
38. Shatzel JJ, Olson SR, Tao DL, McCarty OJT, Danilov AV, DeLoughery TG. Ibrutinib-associated bleeding: pathogenesis, management and risk reduction strategies. *J Thromb Haemost*. 2017;15(5):835-847.
39. Joseph RE, Amatya N, Fulton DB, Engen JR, Wales TE, Andreotti A. Differential impact of BTK active site inhibitors on the conformational state of full-length BTK. *Elife*. 2020;9:e60470.
40. Dhami K, Chakraborty A, Gururaja TL, et al. Kinase-deficient BTK mutants confer ibrutinib resistance through activation of the kinase HCK. *Sci Signal*. 2022;15(736): eabg5216.